Check for updates

A novel dihydro phenylquinazolinone-based two-in-one colourimetric chemosensor for nickel(II), copper(II) and its copper complex for the fluorescent colourimetric nanomolar detection of the cyanide anion†

Meman Sahu,[a] Amit Kumar Manna,[a] Shubhamoy Chowdhury[b] and Goutam Kumar Patra [ID] *[a]

Currently, considerable efforts have been devoted to the detection and quantification of hazardous multi-analytes using a single probe. Herein, we have developed a simple, environment-friendly colourimetric sensor for the sensitive, selective and rapid detection of Ni^{2+} and Cu^{2+} ions using a simple organic Schiff base ligand **L** in methanol–Tris–HCl buffer (1 : 1 v/v, 10 mM, pH = 7.2). The probe **L** exhibited a binding-induced colour change from colourless to yellow and fluorescence quenching in the presence of both Ni^{2+} and Cu^{2+} ions. The interactions between **L** and the respective metal ions were studied by Job's plot, electrospray ionisation-mass spectrometry (ESI-MS), Fourier-transform infrared spectroscopy (FT-IR), density functional theory (DFT) and time-dependent density functional theory (TDDFT) calculations. The limit of detection (LOD) of **L** towards Ni^{2+} and Cu^{2+} was calculated to be 7.4×10^{-7} M and 4.9×10^{-7} M, respectively. Furthermore, the $L–Cu^{2+}$ complex could be used as a new cascade fluorescent-colourimetric sensor to detect CN^- ions with a very low level of detection (40 nM). Additionally, **L** could operate in a wide pH range, and thus was successfully applied for the detection and quantification of Ni^{2+} and Cu^{2+} in environmental samples, and for building OR- and IMPLICATION-type logic gates.

Introduction

Presently, the design and synthesis of smart organic molecules for use as chemosensors with high selectivity and sensitivity towards metal cations and anions have attracted substantial attention.[1,2] These sensors exploit the colourimetric and fluorescent properties of organic molecules, which are applied in analytical, biomedical and environmental sciences.[3–5] Optical methods based on colourimetric receptors are especially attractive due to their real-time analysis, simplicity, and low cost in comparison to other closely related processes such as fluorescence, where UV radiation and sophisticated instruments are required, although the latter is more sensitive than the former.[6–11]

A small amount of Cu^{2+} is required for maintaining good health, but if its concentration is increased, it has a toxic effect on the living body. Cu is the 3rd most important trace element, after Fe and Zn in various biological metabolic processes.[12–14] The free copper commonly found in water is potentially toxic to living organisms and the ecosystem. A high concentration of copper in the body for a short period can cause various serious diseases such as amyotrophic lateral sclerosis,[15] Alzheimer's disease,[16] Parkinson's disease,[17] Wilson's disease[18] and Menkes syndrome.[19] According to the US Environmental Protection Agency, the limit of tolerable concentration of Cu^{2+} ions in drinking water is 20 μM. Hence, researchers are focused on the development of highly selective chemosensors for copper ions.

Ni^{2+}, an essential constituent of several metalloenzymes such as hydrogenases, carbon monoxide dehydrogenases and acireductone deoxygenases, plays a key role in biological processes such as metabolism, respiration and biosynthesis.[20,21] Furthermore, it is widely applied in the manufacture of useful electronics devices in the chemical industry such as Ni–Cd batteries, electroplating, and electroforming.[22,23] Stainless steel is one of the alloys of nickel, which is used in the production of tools, machinery and armaments.[24] However, the excessive accumulation of Ni^{2+} above its prescribed limits has a negative impact on human health, which can cause respiratory problems, lung cancer, pneumonitis, allergies, and central nervous disorders.[25,26] Thus, currently, the precise detection of Ni^{2+} ions

[a]*Department of Chemistry, Guru Ghasidas Vishwavidyalaya, Bilaspur (C.G), India. E-mail: patra29in@yahoo.co.in; Tel: +917587312992*

[b]*Department of Chemistry, Gour Banga University, Malda, West Bengal 732 103, India*

at a biological and environmental level is one of the challenging research interests. There are several reports on the selective recognition of Ni^{2+} and Cu^{2+}.[27–31]

Many state-of-the-art analytical techniques such as atomic absorption spectrometry (AAS),[32] inductively coupled plasma-mass spectroscopy (ICPMS),[33] inductively coupled plasma atomic emission spectrometry (ICP-AES),[34] neutron activation analysis (NAA),[35] anodic stripping voltammetry (ASV),[36] electro-thermal atomic absorption spectrometry (EAAS),[37] chromatography,[38] and cold vapour atomic absorption spectrometry (CVAAS)[39] are employed for the determination of metal ions. However, these methods require expensive instruments, well-controlled experimental conditions, multi-step and complicated sample preparation processes and are time consuming. Some nanoparticle-based chemosensors are also available,[40,41] but they exhibit limitations, such as tedious synthetic protocols, high cost, low durability, and high dependence on external conditions such as pH and irreversibility. Thus, although a large number of fluorescent colourimetric sensors for Cu^{2+} are known, their practical applications are limited due to their slow response, low sensitivity and lack of high selectivity within the cytotoxicity limit.[42–44] Moreover, selective fluorescent colourimetric chemo-sensors for Cu^{2+} ions with a detection limit at the ppb level are rare in the literature.[45,46] Therefore, the development of selective fluorescent colourimetric chemosensors for the fast detection of Cu^{2+} ions in the environment is urgent.

CN^- is well known as one of the most quickly acting and serious poisons, where its toxicity results from its strong affinity to bind to the iron in cytochrome *c* oxidase, interfering with electron transport and resulting in hypoxia. However, despite their toxicity, the use of cyanides as raw materials for the production of synthetic fibres, resins, herbicides and the gold-extraction process is inevitable.[47] Therefore, reliable and efficient ways of detecting the presence of CN^- ions are quite indispensable. During the last few years, a number of efforts have been devoted to designing various chemosensors targeting the detection of cyanides.[48,49] The most attractive approach is the formation of novel colourimetric cyanide receptors, which permit naked-eye detection *via* a simple colour change without the participation of any expensive instruments.[50] However, many receptors for CN^- ions reported thus far have several limitations such as poor selectivity over F^- or OAc^-, and utilization of expensive chemicals, complicated synthesis, and working only in organic media.[51,52] Therefore, the search for successful and selective cyanide-sensing systems in aqueous environments is still required.

The development of chemosensors that can recognize both metal ions and anions simultaneously is one of the most significant tasks because of their potential applications in the biological field and environmental processes.[53] In addition, the detection of multiple targets with a single receptor will be more efficient and simultaneously less expensive than a one-to-one analysis method, and therefore, would attract more attention.[54] Among the various approaches for the detection of both metal ions and anions, fluorometric and colourimetric methods are very popular because of their high sensitivities, easy operation, rapid response rates and relatively low costs. There are several reports on chemosensors based on rhodamine, coumarin, calixarene, pyrene, 8-hydroxyquinoline, anthraquinone, salicyldehyde, naphthaldehyde and other Schiff base molecules for the sequential detection of Cu^{2+} and CN^-.[55,56] However, their poor water-solubility, laborious synthetic processes, interference from other common metal ions, low detection limit and slow detection in practical applications are some of the serious disadvantages associated with these sensor molecules. In addition, they are generally expensive and not suitable for the fabrication of sensing devices.

Dihydro phenylquinazolinone derivatives are an important class of compounds as inhibitors of cell multiplication and well known as antiarthritic and antispermatogenic drugs.[57,58] Herein, in continuation of our ongoing research on the recognition of different analytes using simple chemosensors,[59–61] we report a simple, easy to prepare, and cost effective colourimetric chemo-sensor, 3-[(E)-(2-hydroxybenzylidene)amino]-1,2-dihydro-2-phenylquinazolin-4(3H)-one (**L**), for the sensitive and selective detection of Ni^{2+} and Cu^{2+} ions and its copper complex for both the colourimetric and fluorometric detection of CN^- ions. The chemosensor **L** detected the presence of the cations Ni^{2+} and Cu^{2+} by both fluorescence quenching and an instant change in colour from colourless to yellow, and its Cu^{2+} complex detected CN^- ions by fluorescence enhancement and colour change from yellow to colourless. The sensor was successfully applied for the detection of Ni^{2+} and Cu^{2+} in environmental samples. In addition, the obtained **L**–Cu^{2+} complex could be used as a new cascade sensor to further detect CN^- through a Cu^{2+} displacement approach.

Experimental

General information

All the required materials used for the synthesis were obtained from Sigma-Aldrich and directly used. Analytical grade solvents were used for all the experiments and freshly prepared double-deionized water was used for dilution and preparing Tris–HCl buffer (10 μM, pH = 7.2) solution. The metal ion solutions were prepared from their nitrate salts. ^1H NMR and ^{13}C NMR spectra were recorded on a Bruker DRX spectrometer operating at 400 MHz in DMSO-d_6 solvent and chemical shifts were recorded in ppm relative to TMS. Absorption spectra were recorded on a Shimadzu UV 1800 spectrophotometer using 10 mm path length quartz cuvettes with a wavelength in the range of 200–800 nm. High-resolution mass (HRms) spectra were recorded on a waters mass spectrometer using the mixed solvent of HPLC methanol and triple distilled water. pH measurements were performed using a digital pH meter (Merck) by adjusting dilute hydrochloric acid and sodium hydroxide in buffer solution. Solutions of the receptor **L** (1×10^{-5} M) and metal salts (1×10^{-4} M) were prepared in methanol–Tris–HCl buffer (10 mM, pH 7.2) medium (1 : 1 v/v) and H_2O, respectively.

X-ray data collection and structure determination

X-ray single crystal data was collected using MoKα ($\lambda = 0.7107$ Å) radiation on a BRUKER APEX II diffractometer equipped with

Table 1 Crystal data and structure refinement parameters for **L**

CCDC number	2019296
Empirical formula	$C_{20}H_{16}N_4O_2$
Formula weight	344.38
Temperature/K	109.38
Crystal system	Triclinic
Space group	$P\bar{1}$
$a/\text{Å}$	6.8671(6)
$b/\text{Å}$	9.1774(14)
$c/\text{Å}$	14.373(3)
$\alpha/°$	108.299(17)
$\beta/°$	91.374(12)
$\gamma/°$	94.052(10)
Volume/Å^3	856.8(3)
Z	2
$\rho_{calc}\text{g/cm}^3$	1.3347
μ/mm^{-1}	0.089
$F(000)$	360.2
Crystal size/mm^3	$0.18 \times 0.16 \times 0.14$
Radiation	Mo Kα ($\lambda = 0.71073$)
2Θ range for data collection/°	4.7 to 49.96
Index ranges	$-7 \leq h \leq 7, -10 \leq k \leq 9, -15 \leq l \leq 12$
Reflections collected	2595
Independent reflections	1639 [$R_{int} = 0.0336, R_{sigma} = 0.0626$]
Data/restraints/parameters	1639/0/236
Goodness-of-fit on F^2	1.049
Final R indexes [$I \geq 2\sigma(I)$]	$R_1 = 0.0469, wR_2 = 0.0911$
Final R indexes [all data]	$R_1 = 0.0718, wR_2 = 0.1048$
Largest diff. peak/hole/e Å^{-3}	0.19/−0.24

a CCD area detector. Data collection, data reduction, and structure solution/refinement were carried out using the software package of SMART APEX.[62] The structures were solved by direct methods (SHELXS-97) and standard Fourier techniques, and refined on F2 using the full matrix least squares procedure (SHELXL-97) using the SHELX-97 package[63] incorporated in WinGX.[64] In most cases, non-hydrogen atoms were treated anisotropically. Hydrogen atoms were fixed geometrically at their calculated positions following the riding atom model. The crystallographic data of 3-[(E)-(2-hydroxybenzylidene)amino]-2-phenylquinazolin-4(3H)-one (**L**) is listed in Table 1. Structural information of **L** has been deposited at the Cambridge Crystallographic Data Center (CCDC number 2019296).

Synthesis of 3-[(E)-(2-hydroxybenzylidene)amino]-1,2-dihydro-2-phenylquinazolin-4(3H)-one (L)

Briefly, 0.302 g (2 mmol) of 2-aminobenzohydrazide was dissolved in 20 mL of dehydrated methanol and 0.214 g (2 mmol) of pyridine 2-carboxaldehyde and 0.244 g (2 mmol) of salicylaldehyde were added dropwise with constant stirring. Then the reaction mixture was refluxed for 8 h under dry conditions. Subsequently, the reaction mixture was kept in air to allow the solvent to evaporate, leaving a colourless solid. Yield, 0.295 g, 85%. Anal. calc. for $C_{20}H_{16}N_4O_2$: C, 69.76; H, 4.68; N, 16.27. Found C, 69.68; H, 4.59; N, 16.36%. EI-MS: m/z 344.3 (**L**, 40%) (Fig. S1†). FTIR/cm^{-1} (KBr): 3620 (−OH) 3295 (−NH), 1698 (vs., C=O), 1652 (vs., C=N) 1512 (Fig. S2†).[1] H NMR (400 MHz,
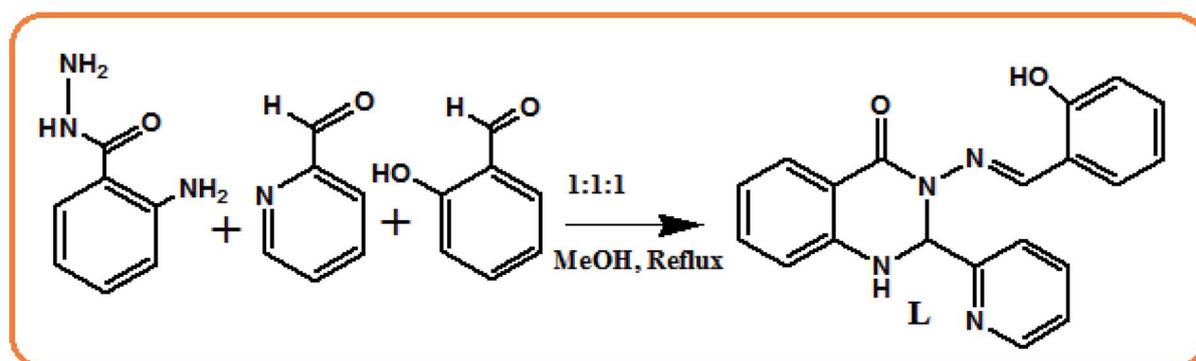
Scheme 1 Synthetic procedure for the synthesis of probe **L**.

DMSO-d_6, TMS): δ 11.57 (s, 1H, –OH), 8.65 (s, 1H, CH=N), 8.48 (s, 1H, –NH), 8.05 (s, 1H), 7.84 (t, 1H), 7.78 (t, 1H), 7.43 (t, 2H), 7.33 (m, 1H), 7.28 (m, 2H), 6.91 (m 2H), 6.78 (m, 3H) (Fig. S3†). ^{13}C NMR (DMSO-d_6, δ ppm, TMS): 160.37, 158.07, 157.81, 149.78, 149.00, 146.36, 137.79, 134.60, 131.98, 130.84, 128.59, 124.28, 121.35, 119.69, 118.97, 118.41, 117.04, 115.26, 114.79, 70.10 (Fig. S4†).

Preparation of stock solution for photophysical measurements

A solution of receptor **L** was prepared initially at the concentration of 1×10^{-3} M in 10 mL in methanol–Tris–HCl buffer medium (10 mM, pH 7.2) solution (1 : 1 v/v), and then diluted to the desired concentration. Also, the stock solution of guest ions were prepared separately from their nitrate salts (except sulphate salt of Mn^{2+} and Fe^{2+}) at a concentration of 1×10^{-3} M in 10 mL double-deionised water and further diluted to their desired concentration. After mixing **L** with each of the metal ions for a few seconds, their absorption and fluorescence spectra were measured at room temperature.

Computational details

All computations were performed using the GAUSSIAN-09 Revision C.01 program software package.[65] Becke's three-parameter hybrid exchange functional and the Lee-Yang-Parr non-local correlation functional (B3LYP)[66] were used throughout this study. Elements besides Cu and Ni were assigned using the 6-31++G** basis set[67] during the calculations. For Cu and Ni, the LanL2DZ[68] basis set was employed. The gas phase geometries of the molecules **L**, [NiL(OH)] (**1**) and [CuL(OCH₃)] (**2**) were optimized fully, unrestricted by the

Table 2 Selected bond parameters for the X-ray structure and geometry-optimized structure of **L**

Bond Parameter	Experimental (L)	Optimized (L)
Bond length (Å)		
O001–C00A	1.221(3)	1.22172
O002–C00G	1.360(4)	1.34509
N003–C008	1.455(4)	1.45888
N003–C00B	1.390(4)	1.39288
N004–N005	1.382(3)	1.35987
N004–C008	1.465(4)	1.46278
N004–C00A	1.385(4)	1.41084
N005–C00H	1.286(4)	1.29096
N006–C00I	1.341(7)	1.33770
N006–C007	1.335(5)	1.33887
Bond angle (°)		
C008–N003–C00B	116.6(2)	119.32339
N005–N004–C008	121.8(2)	121.25606
N005–N004–C00A	114.5(2)	114.45949
C008 –N004–C00A	120.9(2)	122.93190
N004–N005–C00H	121.5(2)	123.62482
C007–N006–C00I	117.5(3)	118.05223
N006–C007–C008	117.3(3)	116.82784
N004–C008–C007	112.0(3)	112.62709
N003–C008–N004	107.1(2)	108.87315
O001–C00A-N004	122.0(3)	121.15673
N004–C00A-C00C	114.1(2)	115.12258
N003–C00B-C00C	118.6(3)	118.60807
N003–C00B-C00K	121.0(3)	121.68903

symmetry in the singlet, doublet and singlet ground states, respectively. The electronic spectra of molecules **L**, **1** and **2** were calculated with the TD-DFT method, and the solvent effect (in
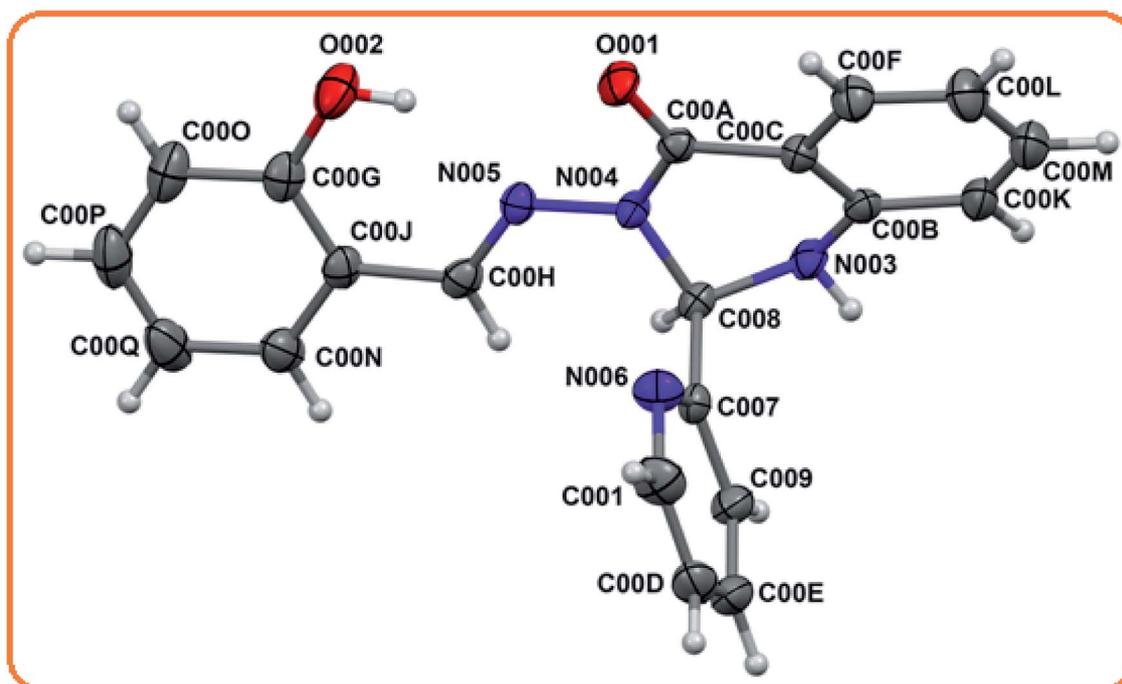

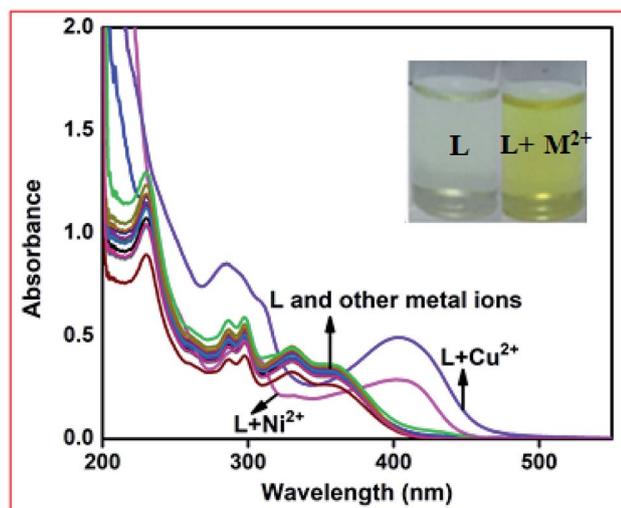**Fig. 1** X-ray crystal structure of **L** with the thermal ellipsoids at 30% probability.

Fig. 2 Changes in the absorption spectra of L (40 µM) in the presence of 5 equiv. of different metal ions. Inset: colour change of L upon the addition of 5 equiv. of Ni²⁺ and Cu²⁺ ions.

methanol) was simulated using the polarizing continuum model with the integral equation formalism (C-PCM).[69,70]

Results and discussion

Synthesis and structure of L

Receptor **L** was synthesized *via* the combination of 2 amino benzohydrazide with either the initial addition of salicylaldehyde followed by pyridine 2 aldehyde or in the reverse order, with high yields (Scheme 1) and characterised by elemental analysis, ¹H-NMR, ESI-MS and FTIR spectroscopy. Its structure was determined by X-ray crystallography. **L** crystallised in the triclinic *P*1 space group.

The molecular structural view of **L** and its atom labeling scheme are shown in Fig. 1. Selected structural parameters are presented in Table 1. The optimization starting from the crystallographically determined molecular structures of **L** led to a minimum as the stationary level. The experimental values of the bonds and angles of **L** are tabulated in Table 2, which are in excellent agreement with the calculated values. The bond lengths differ by less than 0.025 Å, whereas the angles by less than 3°. Thus, the general features noticeable in the experimental data were well reproduced in our calculations.

UV-Vis spectroscopic studies of L towards different metal ions

Initially, the metal selectivity of the proposed receptor was tested *via* absorption spectroscopy in methanol–Tris–HCl buffer (1 : 1 v/v, 10 mM, pH = 7.2) solution. The free receptor **L** produced absorption maxima at 295, 330 and 358 nm, which were almost consistent in the presence of 5 equiv. of different metal ions such as Fe^{3+}, Co^{2+}, Zn^{2+}, Cd^{2+}, Hg^{2+}, Pb^{2+}, Cr^{3+}, Ag^+, Al^{3+}, Mn^{2+}, Pd^{2+}, Pt^{2+}, and Fe^{2+}. Only in the presence of 5 equiv. Ni^{2+} and Cu^{2+} ions in the receptor solution, a red-shifted band appeared at 408 nm for Ni^{2+} and 405 nm for Cu^{2+} together with a change in colour from colourless to yellow for both cases (Fig. 2). This observation preliminary indicates that the receptor shows selective interactions with Ni^{2+} and Cu^{2+} ions.

Next, to determine the details of the sensing process of **L** towards Ni^{2+} and Cu^{2+} ions, absorption titration experiments were conducted in a methanol–Tris–HCl buffer (1 : 1 v/v, 10 mM, pH = 7.2) mixture. Here, the receptor showed an absorption band at 295 nm due to the π–π* transition and n–π* transition at 330 and 358 nm, respectively. Upon the gradual addition of Ni^{2+} and Cu^{2+} ions individually, the absorption band at 408 nm and 405 nm progressively increased and remain constant up to 2 equiv. for Ni^{2+} and 3 equiv. for Cu^{2+}. A well-defined isosbestic point at 373 nm in both the cases was
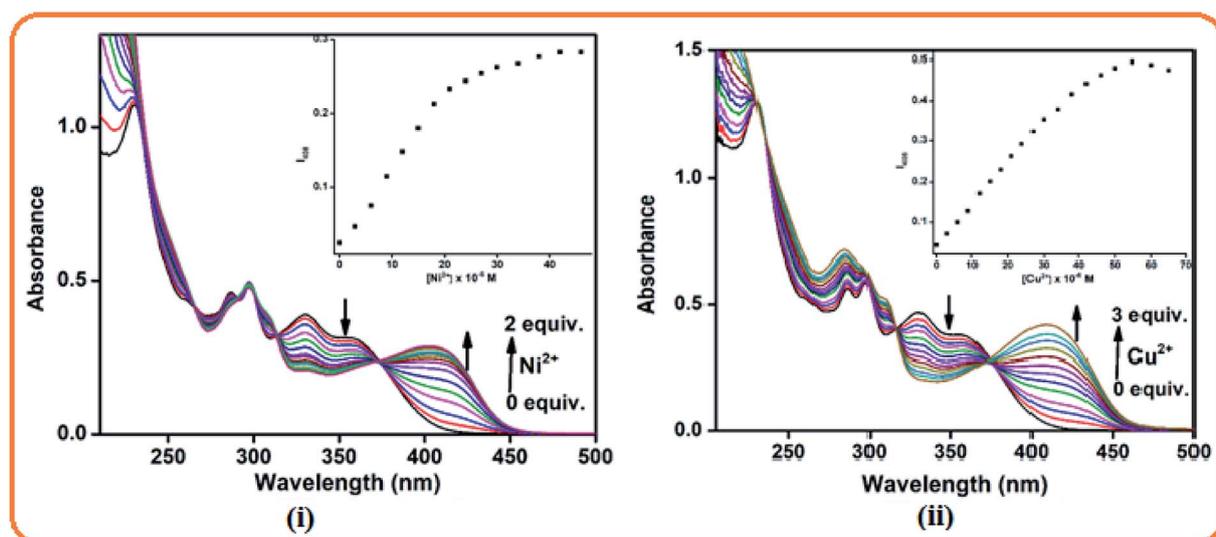

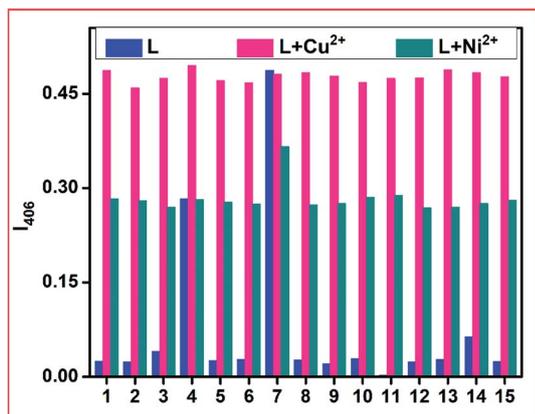Fig. 3 Absorption titration of L towards (i) Ni²⁺ (2 equiv.) and (ii) Cu²⁺ ions (3 equiv.).

Fig. 4 Competitive experiment in the presence of L and other metal ions (where $1 = L$, $2 = Fe^{3+}$, $3 = Fe^{2+}$, $4 = Ni^{2+}$, $5 = Cd^{2+}$, $6 = Co^{2+}$, $7 = Cu^{2+}$, $8 = Hg^{2+}$, $9 = Ag^+$, $10 = Zn^{2+}$, $11 = Pb^{2+}$ $12 = Al^{3+}$, $13 = Cr^{3+}$, $14 = Pd^{2+}$, and $15 = Mn^{2+}$).

observed since dynamic equilibrium exists between L and the L + M^{2+} complexes (M^{2+} = Ni and Cu) in the medium (Fig. 3).

The specific Ni^{2+} and Cu^{2+} ion-selective colourimetric responses of chemosensor L were also studied through competitive experiments. Here, the co-existence of other background cations with Ni^{2+} and Cu^{2+} ions individually did not disturb the absorption band of L + Ni^{2+} and L + Cu^{2+} up to a 3-fold higher level of interfering ions (Fig. 4). Between Ni^{2+} and Cu^{2+} ions, the addition of the same equiv. of Cu^{2+} ions to the L + Ni^{2+} complex solution caused an almost similar peak as that for L + Cu^{2+} to appear due to the displacement of Ni^{2+} from the L + Ni^{2+} complex by Cu^{2+} ions.

The detection limits were calculated from the titration data using the formula $D_L = 3\sigma/m$, where 'σ' is the standard deviation of the blank and 'm' is the slope of the linear calibration curve. The obtained detection limit values for Ni^{2+} and Cu^{2+} were $7.4 \times$

10^{-7} M and 4.9×10^{-7} M, respectively, and thus their detection can be feasible down to a very lower limit (Fig. 5), and the corresponding LOQ values are 2.46×10^{-6} and 1.63×10^{-6}, respectively. According to the Job's plot analysis, the maximum absorption intensity obtained at 0.5 mole fraction of L is due to 1 : 1 binding for both metal ions Ni^{2+} and Cu^{2+} (Fig. S5†). The association constant values for Ni^{2+} and Cu^{2+} were also calculated to be 1.7×10^4 M^{-1} and 1.4×10^3 M^{-1} from the linear fitting of the Benesi–Hildebrand (B–H) graph $1/(A - A_0)$ vs. $1/[M^{2+}]$ (where M^{2+} = Ni and Cu), where 1 : 1 host–guest binding interactions occur (Fig. S6†). The higher association constant of Ni^{2+} ions than Cu^{2+} indicates that at a lower concentration level, Ni^{2+} showed stronger affinity, whereas at a higher concentration level, Cu^{2+} ions showed strong affinity towards L, and thus could replace Ni^{2+} in L + Ni^{2+}.

pH dependence of L, L + Ni^{2+} and L + Cu^{2+}

The metal ion capturing capacity of the proposed chemosensor L is dependent on the pH of the working medium since this receptor contains multiple pH-sensitive moieties. A wide range of receptor solutions with pH values in the range of 3 to 12 were prepared using dil. HCl and NaOH in methanolic medium and the absorption spectra were measured in the presence of the respective metal ions. With an increase in the basicity of the medium, the absorbance intensity of the free receptor and its respective metal complex progressively increased due to the better electrostatic interaction present between the deprotonated form of L and the analytes Ni^{2+} and Cu^{2+} ions (Fig. 6).

Stoichiometry and binding-sites

To ascertain the stoichiometry of both complexes, Job's plots were plotted between mole-fraction X_M and absorbance intensity at 406 nm for both Ni^{2+} and Cu^{2+}. It indicated 1 : 1 (mole ratio) binding of probe L with the metal in each complex, 1 and 2 (vide supra, Fig. S5†). The stoichiometry of both complexes was
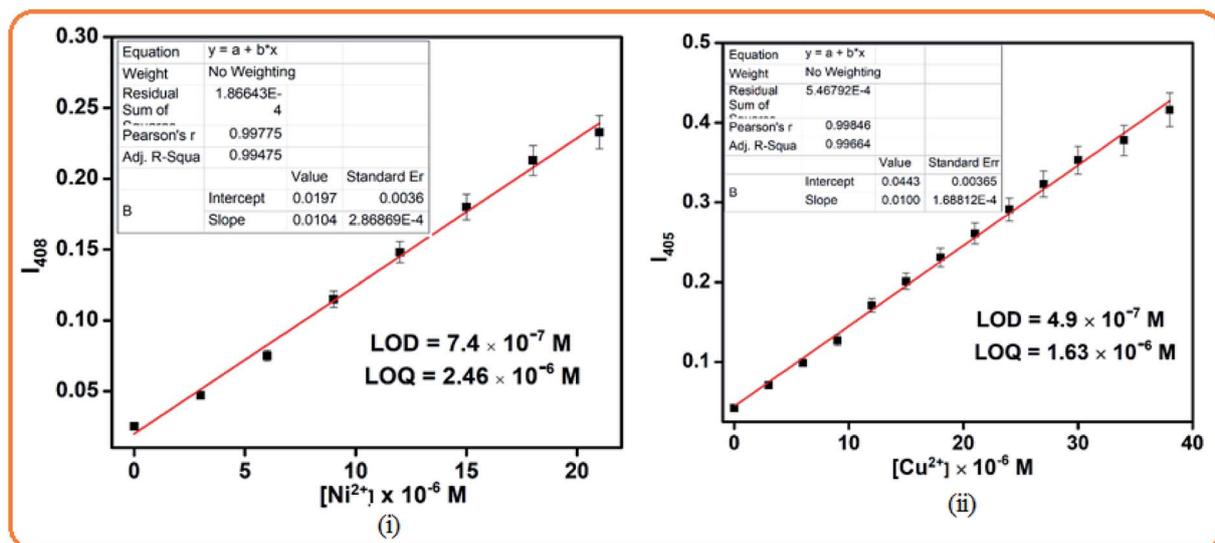

Fig. 5 Detection limits of L towards (i) Ni^{2+} and (ii) Cu^{2+} ions.
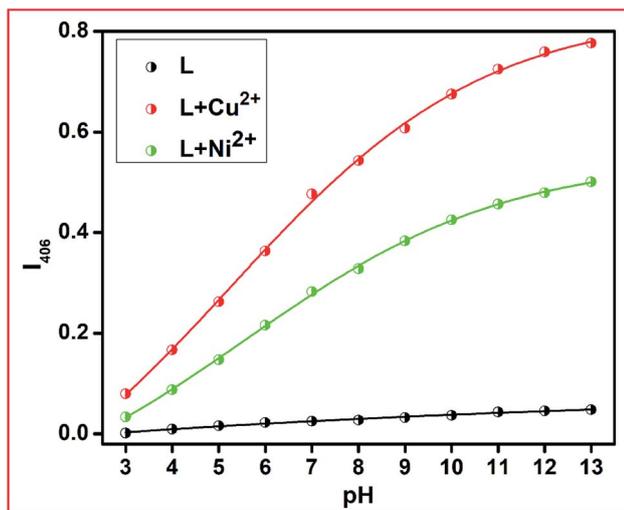
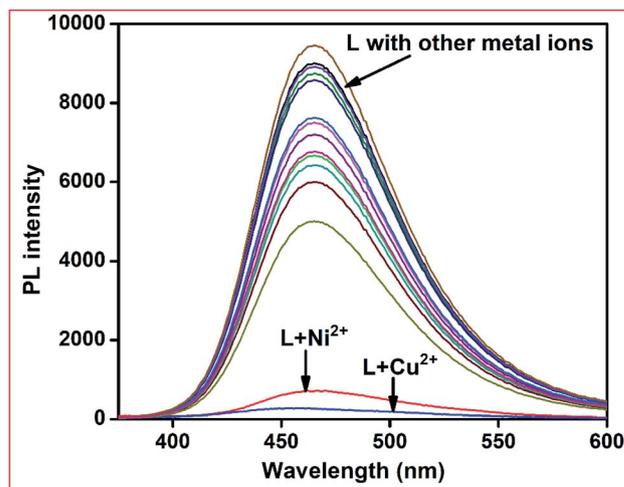**Fig. 6** pH effect of **L** and **L**–M^{2+} complexes (M = Ni^{2+} and Cu^{2+}).

Fig. 7 Fluorescence spectra of **L** in the presence of 5 equiv. of different metal ions in methanol–Tris–HCl buffer (1 : 1 v/v, 10 mM, pH 7.2) solution.

also well corroborated by ESI-MS spectra, where the molecular ion peaks at $m/z = 437.95$ and at $m/z = 419.07$ correspond to **L** + Cu^{2+} + OCH_3–H^+ and **L** + Ni^{2+} + OH–H^+, respectively (Fig. S7†).

The binding of probe **L** with Ni^{2+} and Cu^{2+} was also supported by FT-IR measurements (Fig. S8†). The diagnostic experimental and calculated (non-scaled) IR frequencies of **L**, **1** and **2** and their assignments are listed in Table 3. The calculated vibrational stretching frequencies of **L**, **1** and **2** are in good agreement with the experimentally observed data. Both the experimental and calculated IR spectra of **L**, **1** and **2** are similar in terms of their band positions, band intensities, and shapes of the bands. For **L**, **1** and **2**, the maximum deviations of the calculated IR frequencies vary with their respective

experimental values by less than 10%. These variations are reasonable since the theoretical calculations are based on the gas phase. Also, the theoretically calculated data generally vary with the experimental data.

Fluorescence studies

The emission selectivity of chemosensor **L** towards metal ions was checked in methanol–Tris–HCl buffer (1 : 1 v/v, 10 mM, pH 7.2) solution. When excited at 390 nm, receptor **L** produced an intense emission band at 460 nm due to its rigid structure. Upon the addition of 2 equiv. of several metal ions, only Ni^{2+} and Cu^{2+} showed total fluorescence quenching. The other metal ions including Fe^{3+}, Co^{2+}, Zn^{2+}, Cd^{2+}, Hg^{2+}, Pb^{2+}, Cr^{3+}, Ag^+, Al^{3+}, Mn^{2+}, Pd^{2+}, Pt^{2+}, and Fe^{2+} showed partial quenching of the

Table 3 The diagnostic experimental and calculated IR frequencies are shown for **L**, [NiL(OH)] (**1**) and [CuL(OCH_3)] (**2**)

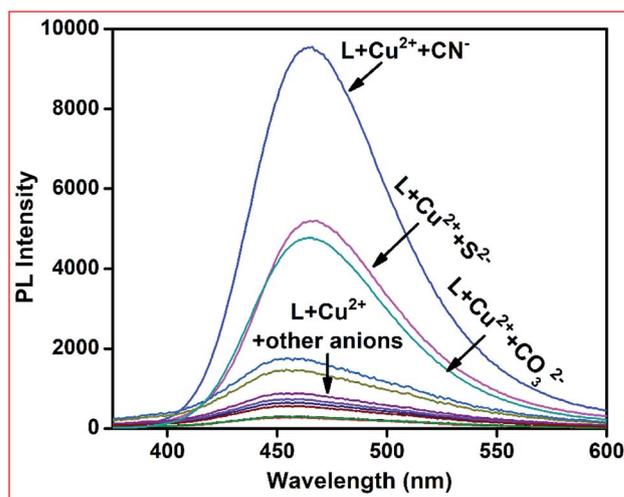| Experimental (cm^{-1})	Theoretical (cm^{-1})	Assignments
L		
	3370.87	$\nu_{(OH)}$
3295	3312.62	$\nu_{(NH)}$
	1533.31	$\delta_{(NH)}$
1698	1725.93	$\nu_{(C=O)}$
1652	1667.80	$\nu_{(C=N)}$
[CuL(OCH_3)] (2)		
3300	3318.22	$\nu_{(NH)}$
	1538.06	$\delta_{(NH)}$
	2944.49, 2991.49, 2993.76	$\nu_{(CH)}$ of –OCH_3
1650	1668.71	$\nu_{(C=O)}$
1615	1627.84	$\nu_{(C=N)}$
[NiL(OH)](1)		
3735	3820.20	$\nu_{(OH)}$ (coordinated)
3296	3613.47	$\nu_{(NH)}$
	1545.20	$\delta_{(NH)}$
1654	1587.72	$\nu_{(C=O)}$
1610	1659.73	$\nu_{(C=N)}$

Fig. 8 Emission spectra of **L** + Cu^{2+} complex towards various anions in methanol–Ttris–HCl buffer (1 : 1 v/v, 10 mM, pH 7.2) solution, excitation wavelength 390 nm.
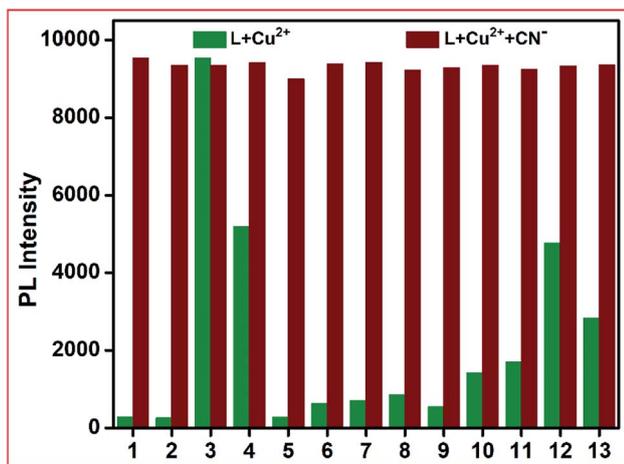
Fig. 9 Emission competitive studies of L + Cu²⁺ + CN⁻ towards various anions (1. HSO₃⁻, 2. OAc⁻, 3. CN⁻, 4. CO₃²⁻, 5. F⁻, 6. Cl⁻, 7. Br⁻, 8. I⁻, 9. H₂PO₄⁻, 10. HCO₃⁻, 11. HF₂⁻, 12. N₃⁻ and 13. S₂⁻).

emission band of the free receptor (Fig. 7). Due to the coordination of the paramagnetic Cu²⁺ and Ni²⁺ ions, electron/energy transfer occurs between the metal ions and fluorophores, and thus fluorescence quenching becomes much more efficient.

L–Cu²⁺ complex to detect anions

The affinity of several anions towards metal ions such as Cu²⁺ and Ni²⁺ ions can be used for anion sensing by further utilising L + M²⁺ (M²⁺ = Cu and Ni) as anion receptors. Thus, we individually prepared L–Cu²⁺ and L–Ni²⁺ complexes *in situ* and their emission spectra were measured in the presence of several anions.

Upon the addition of only CN⁻ ions to the L–Cu²⁺ complex solution, the emission intensity at 460 nm was fully recovered, whereas other anions including HSO₃⁻, OAc⁻, F⁻, Cl⁻, Br⁻, I⁻, H₂PO₄⁻, HCO₃⁻, HF₂⁻, N₃⁻, S²⁻, and CO₃²⁻ did not have a significant influence on the emission spectrum of the L–Cu²⁺ complex (Fig. 8). For the L–Ni²⁺ complex, none of the above-mentioned anions fully recovered the emission intensity, probably due to the lower binding affinity of anions towards Ni²⁺ ions than receptor L.

The specificity of CN⁻ ions towards L–Cu²⁺ was investigated *via* competitive experiments. The emission intensity at 460 nm upon the addition of CN⁻ ions was not altered in the presence of other anions up to a 5-fold higher concentration than that of CN⁻ ions (Fig. 9). These results reveal that the obtained L–Cu²⁺ complex can be used as an efficient fluorescent sensor for recognizing CN⁻, which follows a reversible pathway (Scheme 2). The anion sensing potential of the resultant complex was further investigated *via* fluorescence titration analysis.

In the fluorometric titration experiments, with an increase in the concentration of CN⁻ in the L–Cu²⁺ solution, the emission intensity at 460 nm was gradually enhanced and reached saturation when 5 equiv. of CN⁻ was added. As the concentration of CN⁻ increased, the fluorescence of the L–Cu²⁺ system was restored gradually by a cuprous cyanide precipitation approach due to the stronger affinity of the CN⁻ ion towards Cu²⁺, leading to a prominent fluorescence OFF–ON switching (Fig. 10). Based on the fluorescence titration, the detection limit was calculated to 4.0×10^{-8} M using the formula $D_L = 3\sigma/m$ (Fig. S9†).

The excellent selectivity and sensitivity towards the detection of CN⁻ ions were also observed *via* UV-Vis spectrometry. The colourimetric selective sensing abilities of chemosensor L were investigated *via* UV-Vis absorption spectrometry in methanol–Tris–HCl buffer (1 : 1 v/v, 10 mM, pH 7.2) solution with the abovementioned anions. However, only the addition of cyanide
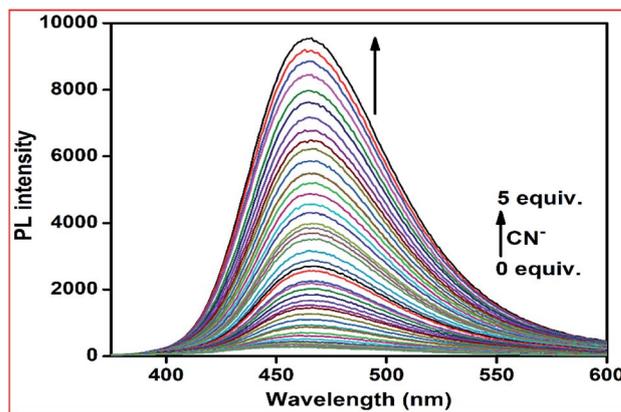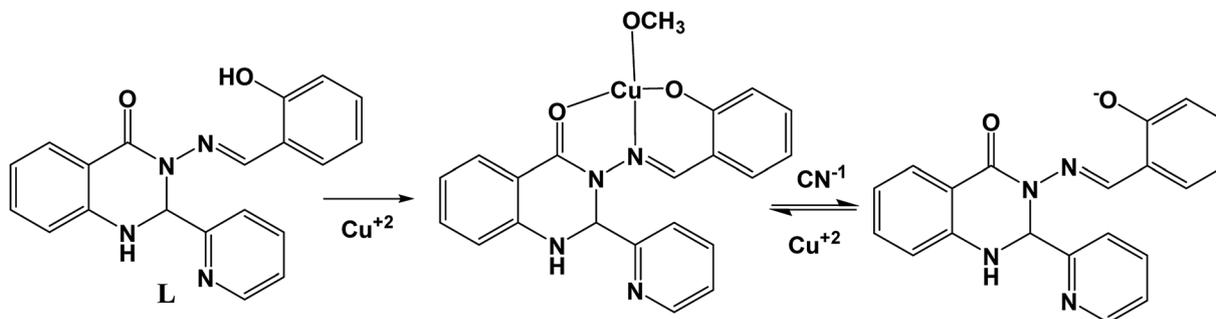

Fig. 10 Fluorescence spectra of L + Cu²⁺ (10 μM) after the addition of increasing amounts of CN⁻ ions (up to 5 equiv.) in methanol–Tris–HCl buffer (1 : 1 v/v) at room temperature (λ_{ex} = 390 nm).

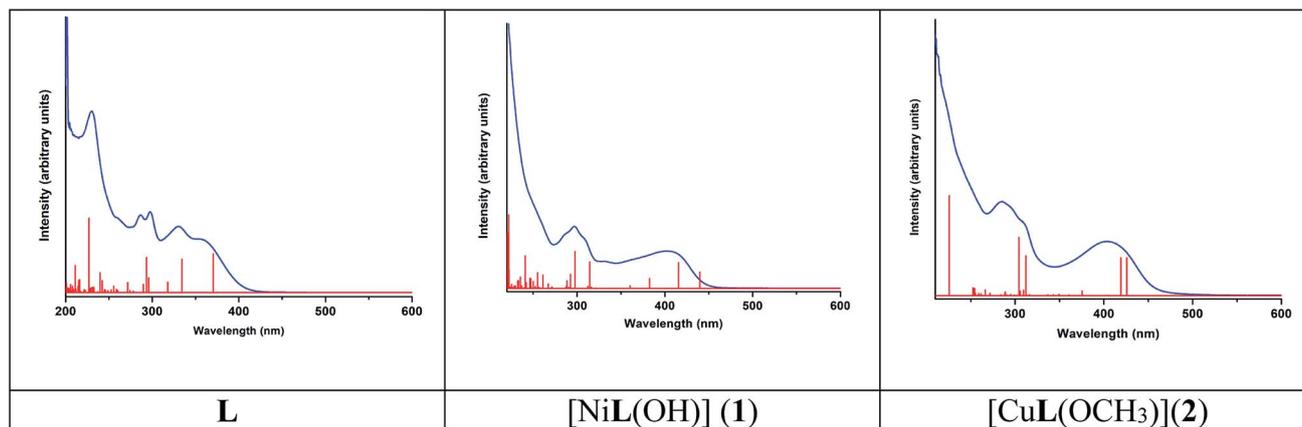Scheme 2 Possible sensing mechanism of L + Cu²⁺ complex for CN⁻.

Fig. 11 Experimental (blue) and calculated electronic transition (red) of L, [NiL(OH)] (**1**) and [CuL(OCH₃)](**2**).

ions induced distinct spectral changes, while the other anions did not induce any spectral change (Fig. S10†).

To examine the reversibility of the receptor **L**–Cu²⁺ complex towards CN⁻ ions, we added hydrochloric acid (HCl, 5 equiv.) to the **L**–Cu²⁺ + CN⁻ guest adduct. Immediately, the fluorescence was quenched and it was further recovered upon the addition of an excess amount of CN⁻ (Fig. S11†). Some recent luminescent

Table 4 Electronic transitions of L, [NiL(OH)] (**1**), and [CuL(OCH₃)] (**2**) calculated in methanol using the TD-DFT method[a]

Most important orbital excitations	λ	f	Experimental λ
L			
H → L	370.43	0.2681	358
H−1 → L	334.32	0.2307	331
H → L+1, H−1 → L+1	317.93	0.0715	
H−2 → L, H → L+2	295.89	0.1005	297
H−2 → L, H−1 → L+1, H → L+2	293.29	0.2416	
H−1 → L+1, H−2 → L, H → L+1, H → L+2	289.78	0.0565	286
H−1 → L+2, H−2 → L, H → L+2	271.74	0.0679	
H−2 → L+1, H−1 → L+3, H−4 → L	255.48	0.0443	
H → L+4, H → L+6, H−5 → L	242.15	0.0816	
H−3 → L+2, H−1 → L+8, H−5 → L+3, H−6 → L+2	216.22	0.0886	230
H−2 → L+4, H → L+12, H−3 → L+3, H → L+10	210.98	0.1861	
H−5 → L+3, H−4 → L+3, H−10 → L, H−6 → L+3	202.25	0.0326	
[NiL(OH)] (1)			
H → L, H−2 → L	439.71	0.1540	
H−1 → L, H−2 → L	415.65	0.2431	406
H−3 → L, H → L+1	382.57	0.0936	
H−4 → L, H−5 → L, H−2 → L+2, H−2 → L+3	314.48	0.2496	
H−2 → L+2, H−4 → L, H−2 → L+1	297.62	0.3489	0.0936
H−3 → L+2, H−5 → L, H−3 → L+1	293.10	0.0045	0.2496
H−4 → L+2, H−9 → L, H−5 → L+2	261.15	0.1255	0.3489
H → L+5, H−9 → L, H → L+6	255.97	0.0130	0.0045
H−7 → L+1, H−6 → L+1, H−5 → L+1	239.87	0.0059	
H−2 → L+6, H−1 → L+6, H → L+12	222.54	0.1783	
[CuL(OCH₃)](2)			
H → L, H−4 → L, H → L+1, H−11 → L,	425.86	0.3357	405
H → L, H−4 → L, H → L+1, H−11 → L	419.22	0.3366	
H−1 → L, H−1 → L+1, H → L+1	375.56	0.0413	
H−4 → L, H−1 → L+1, H−3 → L+1, H → L+2, H → L+3	312.16	0.3531	
H−1 → L+2, H → L+2, H−1 → L+3, H−5 → L+1	305.63	0.0392	306
H−1 → L+2, H → L+3, H−1 → L+3, H−2 → L+2	288.97	0.0323	285
H−8 → L, H−10 → L, H−8 → L+1, H−11 → L	254.32	0.0643	
H → L+6, H → L+5, H → L+8, H → L+5	225.86	0.9054	220sh

[a] λ – wavelength (nm); f – oscillator strength; H – highest occupied molecular orbital; and L – lowest unoccupied molecular orbital.

chemical sensors for the detection and quantification of CN^- in aqueous medium are compiled in Table S1.†

Here, it should be mentioned that the metal complexing indicator displacement approach (IDA) is one of the simplest techniques used for detection of cyanide anions. This approach overcomes the major drawbacks of traditional techniques such as the requirement of expensive instruments and trained personal, high detection limits, time consuming procedure and complicated sample preparation process. In the typical IDA approach, first an indicator (chromophore or fluorophore) can reversibly bind to metal ions *via* non-covalent interaction (coordination), and consequently the optical property of the indicator is altered. The stronger coordination ability of analytes to the receptor (metal) centre displaces the indicator and recovers its optical properties. The major advantages of this technique are (1) the in situ-formed metal centre chemoreceptor result in improved water solubility, (2) sensing towards different analytes can be achieved by simply changing the metal ion (receptor) or a change in the binding site of the indicator, (3) avoids complicated synthetic procedures and (4) the probe can show optical (colour or luminescence) changes as a measured signal, which is very simple, cost effective and highly sensitive.

Time responses of L towards Cu^{2+}, Ni^{2+} and of $L + Cu^{2+}$ towards CN^-

The time evolution of receptor **L** in the presence of 5 equiv. of different metals in methanol–Tris–HCl buffer was investigated, as shown in Fig. S12.† The recognition interaction was almost completed after the addition of only 10 equiv. of metal and the

absorption intensity of **L** at 405 nm remained almost the same up to 20 min. A very quick response time (~5 s) was also observed for **L** + Cu^{2+} towards cyanide ions. After the immediate addition of cyanide ions, an emission intensity appeared at 464 nm and it remained quite stable up to 15 min (Fig. S13†).

DFT studies on L and its Ni^{2+} (1) and Cu^{2+} complexes (2)

The optimized structure of **L**, its Ni^{2+} complex [Ni**L**(OH)] (**1**) and Cu^{2+} complex [Cu**L**(OCH$_3$)] (**2**) are shown in Fig. S14,† and their calculated selected bond distances and angles are listed in Table S1.† The computed bond lengths in **1**, Ni1–O001, Ni1–O002, Ni1–O003, and Ni1–N005 are 1.851, 1.913, 1.835, and 1.897 Å, respectively, which are consistent with the typical range of bond lengths reported elsewhere.[71] The bite angles of O001–Ni1–N005, and O002–Ni1–N005 are 95.509° and 83.099°, respectively, for **1**, which are also in the typical range reported earlier.[59] The calculated bond lengths of Cu1–O001, Cu1–O002, Cu1–O003 and Cu1–N005 in **2** are 1.948, 2.093, 1.852, and 2.061 Å, respectively, which are also in the typical range of bond lengths observed for some reported metal complexes.[72] The bite angles of O001–Cu1–N005 and O002–Cu1–N005 are 91.029° and 76.916°, respectively, for **2**, which are consistent with the reported range.[59] The calculated geometries of the probable structures of **1** and **2** are in good agreement with other reported similar structural geometries in the literature.[71,72]

Molecular orbital description and electronic spectra

The absorption spectra of **L**, **1** and **2** were simulated in the presence of the solvent model (methanol) employing the TD-
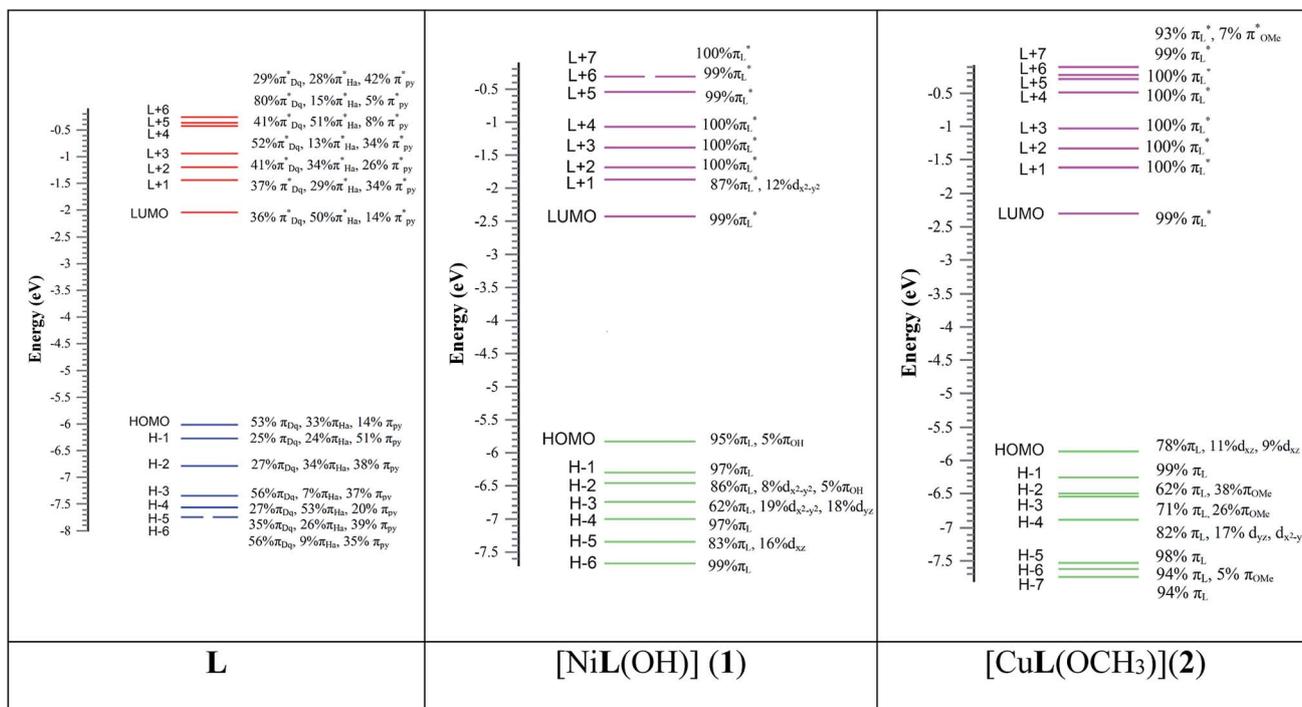

Fig. 12 MO diagrams of **L**, [Ni**L**(OH)] (**1**) and [Cu**L**(OCH$_3$)] (**2**) showing the character and energy (eV) (Ha = (2-hydroxybenzylidene)amino moiety, Py = 2-(pyridin-2-yl) moiety, and Dq = 2,3-dihydroquinazolin-4-one).

DFT methods with the identical basis set and functional as that used in the geometry optimization calculations. The spin-allowed electronic transitions are in good agreement with our experimental data (Fig. 11). The calculated spin-allowed electronic transitions with the experimentally observed data for **L**, **1** and **2** in methanol are summarized in Table 4. The selected
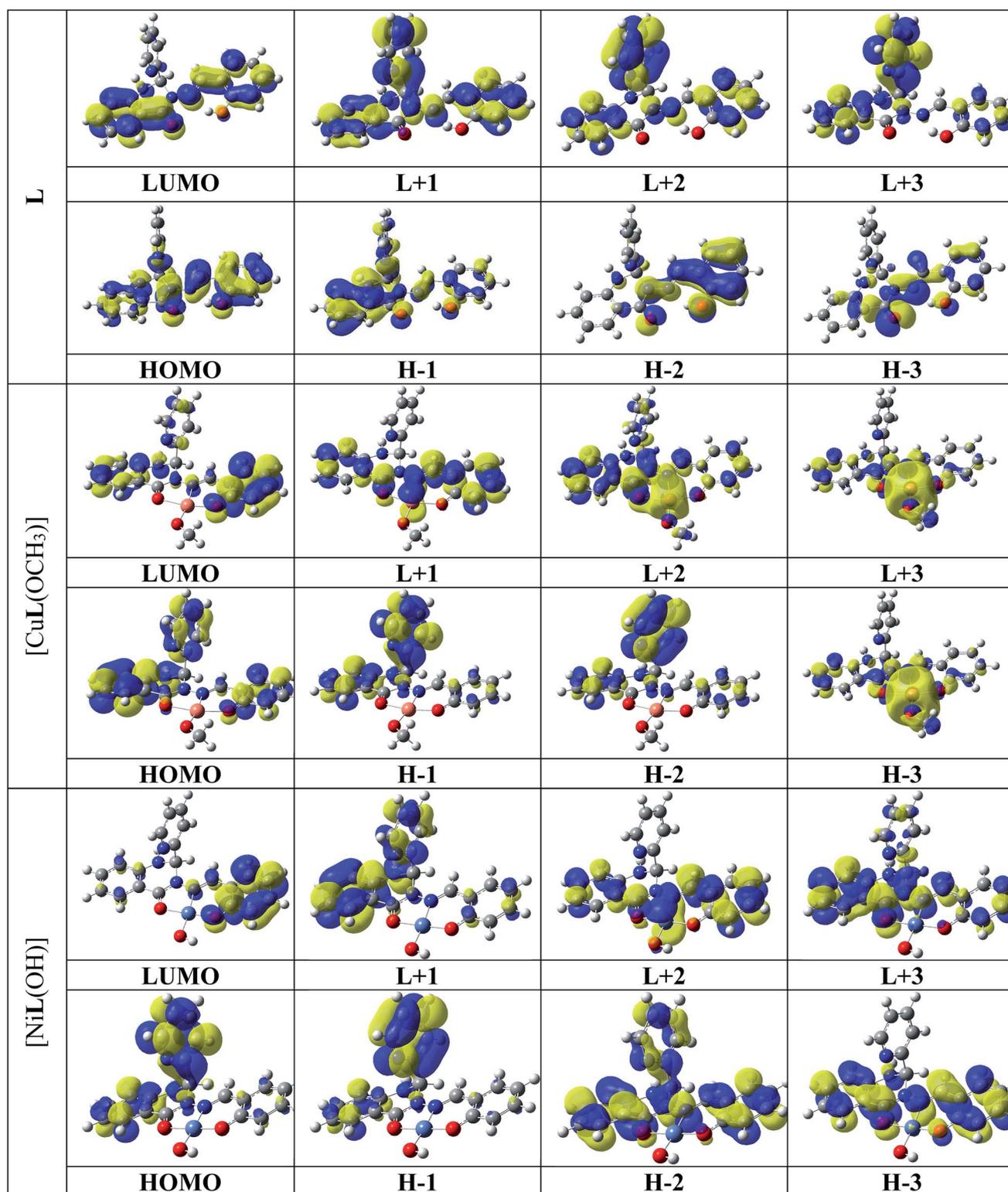

Fig. 13 Selected HOMOs and LUMOs of **L**, [CuL(OCH$_3$)] (**2**), and [NiL(OH)] (**1**). Positive values of the orbital contour are represented in yellow (0.03 a.u.) and negative values in blue (−0.03 a.u.).

transitions of **L**, **1** and **2** having significant oscillator strengths were incorporated and also the transitions with only orbital contributions larger than 8% were considered for the molecules. A schematic representation of the energy of the MOs and contours of selected HOMO and LUMO orbitals of **L**, **1** and **2** are presented in Fig. 12 and 13. The HOMO to LUMO energy gap for **L**, **1** and **2** is 3.976, 3.413 and 3.539 eV, respectively. The energy transition was calculated to be at 370.43 and 334.32 nm for **L**, which can be assigned as n–n* and/or n–π*, respectively. The experimental bands at λ_{max} 358 nm and 330 nm are consistent with the theoretical findings. In the metal complexes, the non-bonded electron ligand **L** binds with the metal, and hence the n–n* and/or n–π* bands are absent or decrease in metal complexes **1** and **2**. Based on the molecular orbital analysis, the other calculated transitions of **L** can be assigned as intra ligand charge transfer transitions. In contrast, the calculated transitions of H → L, H−4 → L, H → L+1, H−11 → L, and H → L,

H−4 → L, H → L+1, H−11 → L at 425.86 and 419.22 nm for **2** is assigned as metal to ligand charge transfer (MLCT) along with some contribution of ligand to ligand charge transfer (LLCT). The rest of the transitions are assigned as intra ligand charge transfer as well as ligand to π orbitals of coordinated OMe molecules transitions. The HOMO levels H and H−4 of **2** have partially metallic in character. Thus the calculated transitions are either of metal to ligand charge transfer (MLCT) or intra ligand charge transfer transitions and ligand to π orbitals of coordinated OMe transitions. Similarly the calculated transitions H → L, H−2 → L; H−1 → L, H−2 → L; and H−3 → L and H → L+1 at 439.71, 415.65, and 382.57 nm for **1** are assigned as the metal to ligand charge transfer (MLCT) beside some contribution of ligand to ligand charge transfer (LLCT). The remaining transitions are assigned as intra ligand charge transfer and ligand to π orbital transitions of the coordinated OH moiety. The calculated bands for **L**, **1** and **2** are in good
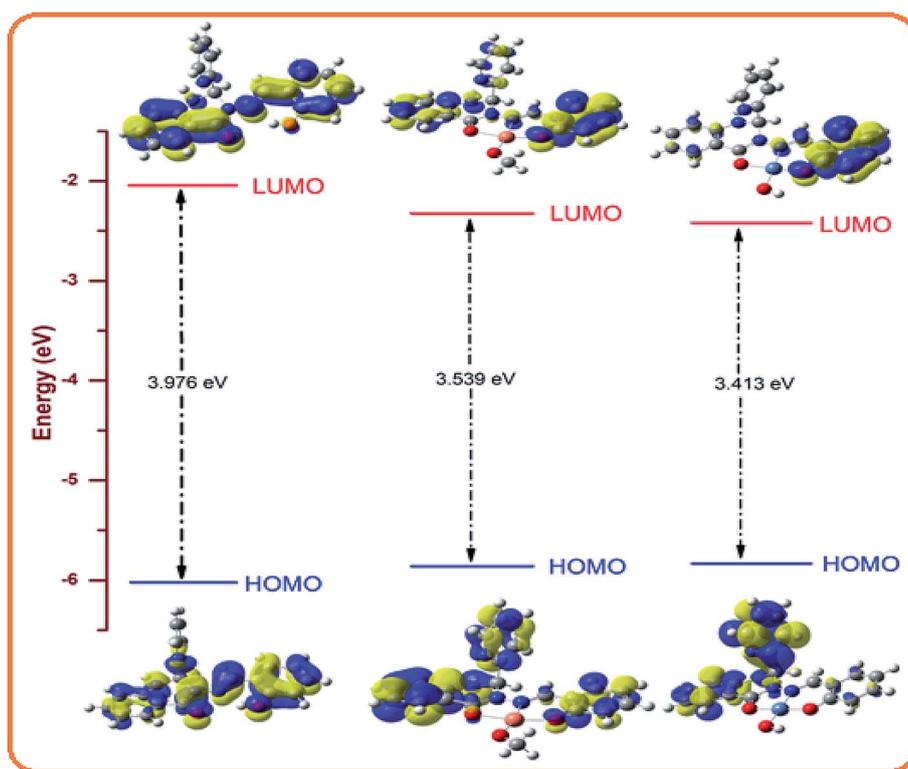
Fig. 14 HOMO−LUMO energy levels of **L**, [CuL(OCH₃)] (**2**) and [NiL(OH)] (**1**).

Table 5 Determination of Ni²⁺ and Cu²⁺ ions in different water samples

Cations	Spiked amount (μM)	Recovered amount (μM)	% recovery ± SD (n = 3)
Ni²⁺	5	5.11	102.2 ± 0.97
	10	9.87	98.7 ± 1.22
	20	19.97	99.8 ± 0.87
Cu²⁺	5	5.08	101.6 ± 0.98
	10	10.15	101.5 ± 0.93
	20	20.07	100.3 ± 1.2

Table 6 Determination of CN$^-$ ions in different water samples

Anion	Spiked amount (μM)	Recovered amount (μM)	% recovery ± SD ($n = 3$)
CN$^-$	5	5.11	102.2 ± 1.15
	10	9.97	99.7 ± 0.93
	20	20.08	100.4 ± 0.89

agreement with the experimentally measured bands in solution and listed in Table 4.

Absorption and fluorescence properties of L, 1 and 2 from DFT

Probe **L** exhibits a simple chelating of metal approach for the selective detection of Ni^{2+} and Cu^{2+} with red shifts in its absorption band due to metal to ligand charge transfer. The energy gap between the highest occupied molecular orbital (HOMO) and lowest unoccupied molecular orbital (LUMO) of **L**, **1** and **2** is 3.976, 3.413 and 3.539 eV, respectively. **1** and **2** compared to **L** are established to exhibit an easy electronic transition, resulting in their further stability (Fig. 14). The contours of the electronic distribution in the HOMO and LUMO states of these molecules suggest significant energy differences of 0.563 and 0.437 eV between **L** and **1** and **2**, respectively.

The fluorescence intensity of the probe diminished because of the chelation and ICT (internal charge transfer) processes after interaction with the Ni^{2+} and Cu^{2+} ions. Specifically, the LUMO states of **1** and **2** compared to that of **L** revealed that the electrons are less delocalized in the **1** and **2** molecules than **L**, in agreement with the barrier of the photoinduced electron transfer process, which may result in a decrease in fluorescence through the chelation of the metal.[73]

Application of chemosensor L in real samples

Chemosensor **L** was successfully applied in the detection of both Ni^{2+} and Cu^{2+} ions in different water samples since normal water resources can be contaminated by Cu^{2+} and Ni^{2+} ions from waste water and the food and chemical industries. Thus, artificial Ni^{2+} and Cu^{2+} ion-contaminated samples were prepared separately by spiking different known concentration levels, and then their concentrations were analysed using the proposed sensing method. The experiment was repeated 3 times with each sample, and good recovery and very low standard deviation were observed, as shown in Table 5.

The CN$^-$ ion sensing ability of the receptor **L**–Cu^{2+} in real water sample was also studied. Accordingly, an artificial CN$^-$-contaminated sample was prepared in tap water and the recovery amount for each concentration of spiked ions was calculated using the calibration curve (Fig. S9†), with the help of Lambert–Beers law. According to the results shown in Table 6, the low recovery amount obtained within the range of 99% to 105% with RSD values of less than 5% signify that the complex probe **L**–Cu^{2+} can be used to detect CN$^-$ ions in real water samples.

Molecular logic gate

The optical behaviour change of receptor **L** in the presence of analytes Ni^{2+} and Cu^{2+} ions can be used for the construction of bimolecular supramolecular logical devices. Supramolecular logic gates are potential candidates for computation at a minimal level with two chemical input and output results based on spectral intensity represented by binary codes 0 and 1. The absorption intensity at 405 nm in the presence of either Cu^{2+}/Ni^{2+} ions or both mimic the construction of an OR logical function with the threshold value of 0.1. On the other hand, the decrease in the emission intensity at 460 nm in the presence of Cu^{2+} ions reappears in the presence of CN$^-$ ion, which can be applicable for IMPLICATION-type logic gate. Both logic gates and their corresponding truth tables are presented in Fig. 15.

Conclusions

In summary, a dihydro phenylquinazolinone-based novel two-in-one colourimetric sensor **L** was designed, synthesized and exploited for the dual detection and quantification of Ni^{2+} and Cu^{2+} ions and displayed an instant colour change from colourless to yellow and fluorescence quenching in the presence of these cations. The colorimetric lowest limit of detection of **L** towards Ni^{2+} and Cu^{2+} was calculated to be 7.4×10^{-7} M and 4.9×10^{-7}, respectively. The **L**–Cu^{2+} complex was also used as a new sequential fluorescent turn-on sensor to detect CN$^-$ ions up to a detection level of 40 nM through a Cu^{2+} displacement approach. Also, **L** could function in a wide pH range and could

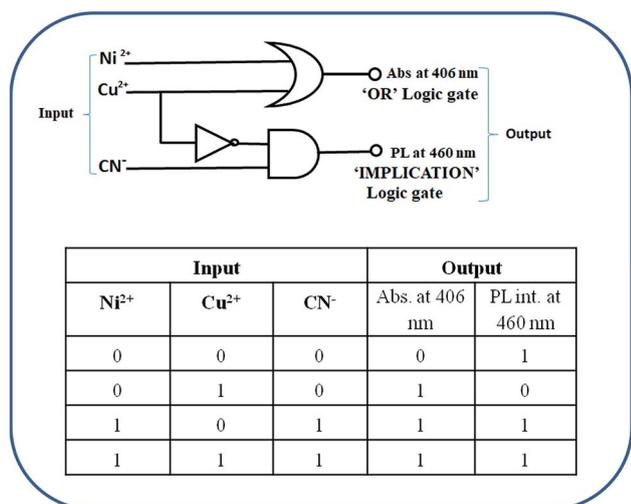|	Input		Output	
Ni^{2+}	Cu^{2+}	CN$^-$	Abs. at 406 nm	PL int. at 460 nm
0	0	0	0	1
0	1	0	1	0
1	0	1	1	1
1	1	1	1	1

Fig. 15 OR and IMPLICATION logic gates and truth table.

be effectively applied for the detection and quantification of Ni^{2+} and Cu^{2+} in various environmental samples, and for building OR and IMPLICATION-type logic gates.

Conflicts of interest

Authors declare no conflicts of interest.

Acknowledgements

References

1 A. L. Berhanu, Gaurav, I. Mohiuddin, A. K. Malik, J. S. Aulakh, V. Kumar and K. H. Kim, A review of the applications of Schiff bases as optical chemical sensors, *TrAC – Trend Anal. Chem.*, 2019, **116**, 74–91.

2 G. Sivaraman, I. Murugan Iniya, T. Anand, N. G. Kotla, O. Sunnapu, S. Singaravadivel, A. Gulyani and D. Chellappa, Chemically diverse small molecule fluorescent chemosensors for copper ion, *Coord. Chem. Rev.*, 2018, **357**, 50–104.

3 A. K. Manna, S. Chowdhury and G. K. Patra, Combined experimental and theoretical studies on a phenyl thiadiazole-based novel turn-on fluorescent colorimetric Schiff base chemosensor for the selective and sensitive detection of Al^{3+}, *New J. Chem.*, 2020, **44**, 10819–10832.

4 S. Wu, H. Min, W. Shi and P. Cheng, Multicenter Metal–Organic Framework-based ratiometric fluorescent sensors, *Adv. Mater.*, 2019, 1805871.

5 S. Ge, J. He, C. Ma, J. Liu, F. Xi and X. Dong, One-step synthesis of boron-doped graphene quantum dots for fluorescent sensors and biosensor, *Talanta*, 2019, **199**, 581–589.

6 P. A. Gale and C. Caltagirone, Fluorescent and colourimetric sensors for anionic species, *Coord. Chem. Rev.*, 2018, **354**, 2–27.

7 V. S. AjayPiriya, J. Printo, S. C. G. Kiruba Daniel, L. Susithra, K. Takatoshi and M. Sivakumar, Colorimetric sensors for rapid detection of various analytes, *Mater. Sci. Eng. C*, 2017, **78**, 1232–1245.

8 T. A. Khattab, M. M. G. Fouda, M. Rehan, M. K. Okla, S. A. Alamri, I. A. Alaraidh, A. A. Al-ghamdi, W. H. Soufand, E. M. Abdelsalam and A. A. Allam, Novel halochromic cellulose nanowhiskers from rice straw: Visual detection of urea, *Carbohydr. Polym.*, 2020, **231**, 115740.

9 N. De Acha, C. Elosúa, J. M. Corres and F. J. Arregui, Fluorescent sensors for the detection of heavy metal ions in aqueous media, *Sensors*, 2019, **19**, 599.

10 T. A. Khattab, From chromic switchable hydrazones to smart materials, *Mater. Chem. Phys.*, 2020, **254**, 123456.

11 M. Denis, J. Pancholi, K. Jobe, M. Watkinson and S. M. Goldup, Chelating rotaxane ligands as fluorescent sensors for metal ions, *Angew. Chem., Int. Ed.*, 2018, **57**, 5310–5314.

12 P. Ghosh, K. Pramanik, S. Paul, P. Malpaharia, S. K. Chandra, S. K. Mukhopadhyay and P. Banerjee, Trace level recognition of Zn^{2+} and Cd^{2+} by biocompatible chemosensor inside androecium, diagnosis of pick's disease from urine and biomimetic β-cell exocytosis, *ACS Appl. Bio Mater.*, 2018, **1**, 683–692.

13 K. P. Carter, A. M. Young and A. E. Palmer, Fluorescent sensors for measuring metal ions in living systems, *Chem. Rev.*, 2014, **114**, 4564–4601.

14 U. Fegade, A. Saini, S. K. Sahoo, N. Singh, R. Bendre and A. Kuwar, 2,2′-(Hydrazine-1,2 diylidenedimethylylidene) bis(6-isopropyl-3-methylphenol) based selective dual-channel chemosensor for Cu^{2+} in semiaqueous media, *RSC Adv.*, 2014, **4**, 39639–39644.

15 A. Umesh, S. Fegade, S. K. Sahoo, A. Singh, N. Singh, S. B. Attarde and A. S. Kuwar, A chemosensor showing discriminating fluorescent response for highly selective and nanomolar detection of Cu^{2+} and Zn^{2+} and its application in molecular logic gate, *Anal. Chim. Acta*, 2015, **872**, 63–69.

16 U. Fegade, H. Sharma, B. Bondhopadhyay, A. Basu, S. Attarde, N. Singh and A. Kuwar, "Turn-on" fluorescent dipodal chemosensor for nano-molar detection of Zn^{2+}: Application in living cells imaging, *Talanta*, 2014, **125**, 418–424.

17 G. Multhaup, A. Schlicksupp, L. Hess, D. Beher, T. Ruppert and C. L. Masters, The amyloid precursor protein of Alzheimer's disease in the reduction of copper (II) to copper (I), *Science*, 1996, **271**, 1406–1409.

18 R. A. Løvstad, A kinetic study on the distribution of Cu (II)-ions between albumin and transferring, *BioMetals*, 2004, **17**, 111–113.

19 Y. H. Hung, A. I. Bush and R. A. Cherny, Copper in the brain and Alzheimer's disease, *J. Biol. Inorg Chem.*, 2010, **15**, 61–76.

20 J. C. Lee, H. B. Gray and J. R. Winkler, Copper (II) binding to α-synuclein, the Parkinson's protein, *J. Am. Chem. Soc.*, 2008, **130**, 6898–6899.

21 E. Madsen and J. D. Gitlin, Copper and iron disorders of the brain, *Annu. Rev. Neurosci.*, 2007, **30**, 317–337.

22 B. Zambelli, F. Musiani, S. Benini and S. Ciurli, Chemistry of Ni^{2+} in Urease: Sensing, Trafficking, and Catalysis, *Acc. Chem. Res.*, 2011, **44**, 520–530.

23 S. W. Ragsdale, Nickel-based Enzyme Systems, *J. Biol. Chem.*, 2009, **284**, 18571–18575.

24 K. S. Kasprzak, F. W. Sunderman and K. Salnikowa, A Bio-assessment of DNA damage by Alkaline Comet Assay in metal workers of Kano metropolis, Nigeria, *Mutat. Res.*, 2003, **533**, 67–97.

25 P. H. Kuck, *Mineral Commodity Summaries: Nickel*, United States Geological Survey, 2006.

26 J. R. Davis, Uses of Nickel, ASM Specialty, *Handbook: Nickel, Cobalt, and Their Alloys*, ASM International, 2000, vol. 7.

27 R. Awual, M. Hasan, J. Iqbal, A. Islam, S. Khandaker, A. M. Asiri and M. M. Rahman, Ligand based sustainable composite material for sensitive nickel(II) capturing in aqueous media, *J. Env. Chem. Eng.*, 2020, **8**, 103591.

28 M. M. Rahman, S. B. Khan, H. M. Marwani and A. M. Asiri, Selective detection of divalent nickel ions based on wet-chemically prepared Cs-doped ZnO nanosheets, *Superlattices Microstruct.*, 2014, **71**, 93–104.

29 S. B. Khan, K. A. Alamry, H. M. Marwani, A. M. Asiri and M. M. Rahman, Synthesis and environmental applications of cellulose/ZrO$_2$ nanohybrid as a selective adsorbent for nickel ion, *Compos. B Eng.*, 2013, **50**, 253–258.

30 M. A. Hasnat, Z. Mumtarin and M. M. Rahman, Electrocatalytic reduction of hydroxylamine on copper immobilized platinum surface: heterogeneous kinetics and sensing performance, *Electrochim. Acta*, 2019, **318**, 486–495.

31 M. R. Awual, M. M. Hasan, M. M. Rahman and A. M. Asiri, Novel composite material for selective copper(II) detection and removal from aqueous media, *J. Mol. Liquids*, 2019, **283**, 772–780.

32 W. Lee, K. A. Davis, R. L. Rettmer and R. F. Labbe, Ascorbic acid status: biochemical and clinical considerations, *Am. J. Clin. Nutr.*, 1988, **48**, 286–290.

33 X. Q. Liu, X. Zhou, X. Shu and J. Zhu, Chain Packing in Electro-Spun Poly(ethylene oxide) Visualized by Atomic Force Microscopy, *Macromolecules*, 2009, **42**, 7634–7636.

34 M. H. Mashhadizadeh, M. Pesteh, M. Talakesh, I. Sheikhshoaie, M. M. Ardakani and M. A. Karimi, Solid phase extraction of copper (II) by sorption on octadecyl silica membrane disk modified with a new Schiff base and determination with atomic absorption spectrometry, *Spectrochim. Acta, Part B*, 2008, **63**, 885–888.

35 C. F. Harrington, S. A. Merson and T. M. D. D'Silva, Determination of mercury in fish by isotope dilution inductively coupled plasma-mass spectrometry, *Anal. Chim. Acta*, 2004, **505**, 247–254.

36 S. L. C. Ferreira, A. S. Queiroz, M. S. Fernandes and H. C. dos Santos, Application of factorial designs and Doehlert matrix in optimization of experimental variables associated with the preconcentration and determination of vanadium and copper in seawater by inductively coupled plasma optical emission spectrometry, *Spectrochim. Acta, Part B*, 2002, **57**, 1939–1950.

37 J. C. Yu, J. M. Lo and K. M. Wai, Extraction of gold and mercury from sea water with bismuth diethyldithiocarbamate prior to neutron activation—γ spectrometry, *Anal. Chim. Acta*, 1983, **154**, 307–312.

38 A. Mohades and M. A. Taher, Voltammetric determination of Cu (II) in natural waters and human hair at a meso-2, 3-dimercaptosuccinic acid self-assembled gold electrode, *Talanta*, 2007, **72**, 95–100.

39 C. Burriniand and A. Cagnini, Determination of mercury in urine by ET-AAS using complexation with dithizone and extraction with cyclohexane, *Talanta*, 1997, **44**, 1219–1223.

40 A. Ali, H. Shen and X. Yin, Simultaneous determination of trace amounts of nickel, copper and mercury by liquid chromatography coupled with flow-injection on-line derivatization and preconcentration, *Anal. Chim. Acta*, 1998, **369**, 215–223.

41 Y. Ma, H. Niu, X. Zhanga and Y. Cai, Colourimetric detection of copper ions in tap water during the synthesis of silver/dopamine nanoparticles, *Chem. Commun.*, 2011, **47**, 12643–12645.

42 N. H. Ly, C. Seo and S.-W. Joo, Detection of copper(II) ions using glycine on hydrazine-adsorbed gold nanoparticles via Raman Spectroscopy, *Sensors*, 2016, **16**, 1785–1795.

43 V. K. Gupta, A. K. Singh and N. Mergu, A new beryllium ion-selective membrane electrode based on dibenzo (perhydrotriazino) aza-14-crown-4 ether, *Anal. Chim. Acta*, 2012, **746**, 44–50.

44 B. J. Sanghavi, S. M. Mobin, P. Mathur, G. K. Lahiri and A. K. Srivastava, Biomimetic sensor for certain catecholamines employing copper (II) complex and silver nanoparticle modified glassy carbon paste electrode, *Biosens. Bioelectron.*, 2013, **39**, 124–132.

45 X. Zhou, S. Lee, Z. Xu and J. Yoon, Recent progress on the development of chemosensors for gases, *Chem. Rev.*, 2015, **115**, 7944–8000.

46 J. J. Lee, Y. W. Choi, G. R. You, S. Y. Lee and C. Kim, A phthalazine-based two-in-one chromogenic receptor for detecting Co^{2+} and Cu^{2+} in an aqueous environment, *Dalton Trans.*, 2015, **44**, 13305–13314.

47 Y. Tsui, S. Devaraj and Y. Yen, Azo dyes featuring with nitrobenzoxadiazole (NBD) unit: a new selective chromogenic and fluorogenic sensor for cyanide ion, *Sens. Actuators, B*, 2012, **161**, 510–519.

48 Q. Lin, X. Liu, T.-B. Wei and Y. M. Zhang, Reaction-Based RatiometricChemosensor for Instant Detection of Cyanide in Water with High Selectivity and Sensitivity, *Chem.–Asian J.*, 2013, **8**, 3015–3021.

49 J. H. Kang, S. Y. Lee, H. M. Ahn and C. Kim, A novel colourimetric chemosensor for the sequential detection of Ni^{2+} and CN$^-$ in aqueous solution, *Sens. Actuators, B*, 2017, **242**, 25–34.

50 S. Park, K. Hong, J. Hong and H. Kim, Azo dye-based latent colourimetric chemodosimeter for the selective detection of cyanides in aqueous buffer, *Sens. Actuators, B*, 2012, **174**, 140–144.

51 J. Kang, E. J. Song, H. Kim, Y. Kim, Y. Kim, S. Kim and C. Kim, Specific naked eye sensing of cyanide by chromogenic host: studies on the effect of solvents, *Tetrahedron Lett.*, 2013, **54**, 1015–1019.

52 Y. Lin, J. Zheng, Y. Tsui and Y. Yen, Colourimetric detection of cyanide with phenyl thiourea-derivatives, *Spectrochim. Acta, Part A*, 2011, **79**, 1552–1558.

53 H. Li, R. A. Lalancette and F. Jäkle, Turn-on fluorescence response upon anion binding to dimesitylboryl-functionalized quaterthiophene, *Chem. Commun.*, 2011, **47**, 9378–9380.

54 A. Liu, L. Yang, Z. Zhang, Z. Zhang and D. Xu, A novel rhodamine-based colourimetric and fluorescent sensor for the dual-channel detection of Cu^{2+} and Fe^{3+} in aqueous solutions, *Dyes Pigm.*, 2013, **99**, 472–479.

55 L. Shang, L. Zhang and S. Dong, Turn-on fluorescent cyanide sensor based on copper ion-modified CdTe quantum dots, *Analyst*, 2009, **134**, 107–113.

56 Z. Xu, X. Chen, H. N. Kim and J. Yoon, Sensors for the optical detection of cyanide ion, *Chem. Soc. Rev.*, 2010, **39**, 127–137.

57 H. J. Yale and M. Kalkstein, Substituted 2,3-dihydro-4(1H)-quinazolinones, a new class of inhibitors of cell multiplication, *J. Med. Chem.*, 1967, **10**, 334–336.

58 G. L. Neil, L. H. Li, H. H. Buskirk and T. E. Moxley, Antitumor effects of the antispermato-genicagent, 2,3-dihydro-2-(1-naphthyl)-4(1H)-quinazolinone (NSC-145669), *Cancer Chemother. Rep.*, 1972, **56**, 163–173.

59 A. K. Manna, J. Mondal, K. Rout and G. K. Patra, A benzohydrazide based two-in-one Ni^{2+}/Cu^{2+} fluorescent colourimetric chemosensor and its applications in real sample analysis and molecular logic gate, *Sens. Actuators, B*, 2018, **275**, 350–358.

60 K. Rout, A. K. Manna, M. Sahu, J. Mondal, S. K. Singh and G. K. Patra, Triazole-based novel bis Schiff base colourimetric and fluorescent turn-on dual chemosensor for Cu^{2+} and Pb^{2+}: application to living cell imaging and molecular logic gates, *RSC Adv.*, 2019, **9**, 25919–25931.

61 R. Chandra, A. K. Manna, K. Rout, J. Mondal and G. K. Patra, A dipodal molecular probe for naked eye detection of trivalent cations (Al^{3+}, Fe^{3+} and Cr^{3+}) in aqueous medium and its applications in real sample analysis and molecular logic gates, *RSC Adv.*, 2018, **8**, 35946–35958.

62 *SMART & SAINT Software Reference manuals, version 5.0*, Bruker AXS Inc., Madison,WI, 1998.

63 T. Gruene, H. W. Hahn, A. V. Luebben, F. Meilleur and G. M. Sheldrick, Refinement of macromolecular structures against neutron data with SHELXL2013, *J. Appl. Cryst*, 2014, **47**, 462–466.

64 L. J. Farrugia, WinGX: An Integrated System of Windows Programs for the Solution, Refinement and Analysis for Single Crystal X-ray Diffraction Data, version 1.80.01, *J. Appl. Crystallogr.*, 1999, **32**, 837–838.

65 M. J. Frisch, G. W. Trucks, H. B. Schlegel, G. E. Scuseria, M. A. Robb, J. R. Cheeseman, G. Scalmani, V. Barone, B. Mennucci, G. A. Petersson, H. Nakatsuji, M. Caricato, X. Li, H. P. Hratchian, A. F. Izmaylov, J. Bloino, G. Zheng, J. L. Sonnenberg, M. Hada, M. Ehara, K. Toyota, R. Fukuda, J. Hasegawa, M. Ishida, T. Nakajima, Y. Honda, O. Kitao, H. Nakai, T. Vreven, J. A. Montgomery Jr, J. E. Peralta, F. Ogliaro, M. Bearpark, J. J. Heyd, E. Brothers, K. N. Kudin, V. N. Staroverov, R. Kobayashi, J. Normand, K. Raghavachari, A. Rendell, J. C. Burant, S. S. Iyengar, J. Tomasi, M. Cossi, N. Rega, J. M. Millam, M. Klene, J. E. Knox, J. B. Cross, V. Bakken, C. Adamo, J. Jaramillo, R. Gomperts, R. E. Stratmann, O. Yazyev, A. J. Austin, R. Cammi, C. Pomelli, J. W. Ochterski, R. L. Martin, K. Morokuma, V. G. Zakrzewski, G. A. Voth, P. Salvador, J. J. Dannenberg, S. Dapprich, A. D. Daniels, Ö. Farkas, J. B. Foresman, J. V. Ortiz, J. Cioslowski and D. J. Fox, *Gaussian 09, Revision C.01*, Gaussian Inc., Wallingford, CT, 2009.

66 A. D. Becke, Density-functional thermochemistry. III. The role of exact exchange, *J. Chem. Phys.*, 1993, **98**, 5648.

67 W. J. Hehre, R. Ditchfield and J. A. Pople, Self—Consistent Molecular Orbital Methods. XII. Further Extensions of Gaussian—Type Basis Sets for Use in Molecular Orbital Studies of Organic Molecules, *J. Chem. Phys.*, 1972, **56**, 2257–2261.

68 P. J. Hay and W. R. Wadt, Ab initio effective core potentials for molecular calculations. Potentials for K to Au including the outermost core orbitals, *J. Chem. Phys.*, 1985, **299**, 82.

69 V. Barone and M. Cossi, Quantum Calculation of Molecular Energies and Energy Gradients in Solution by a Conductor Solvent Model, *J. Phys. Chem. A*, 1995, **102**, 1998–2001.

70 J. Tomasi, B. Mennucci and R. Cammi, Quantum Mechanical Continuum Solvation Models, *Chem. Rev.*, 2005, **105**, 2999–3094.

71 A. Burkhardt, A. Buholz, H. Görls and W. Plass, *Z. Allg. Chem.*, 2003, **639**, 2519–2520.

72 A. K. Manna, J. Mondal, K. Rout and G. K. Patra, A new ICT based Schiff-base chemosensor for colourimetric selective detection of copper and its copper complex for both colourimetric and fluorometric detection of Cysteine, *J. Photochem. Photobiol. A*, 2018, **367**, 74–82.

73 S. Chowdhury, A. Bhattacharya, P. Saha, S. Majumder, E. Suresh and J. P. Naskar, A copper (II) complex of benzimidazole-based ligand: synthesis, structure, redox aspects and fluorescence properties, *J. Coord. Chem.*, 2016, **69**, 3664–3676.